Cell

XBP1 Links ER Stress to Intestinal Inflammation and Confers Genetic Risk for Human Inflammatory Bowel Disease

Arthur Kaser,[1,10,11] Ann-Hwee Lee,[3,10] Andre Franke,[4] Jonathan N. Glickman,[2] Sebastian Zeissig,[1] Herbert Tilg,[5] Edward E.S. Nieuwenhuis,[6] Darren E. Higgins,[7] Stefan Schreiber,[4,9] Laurie H. Glimcher,[3,8,*] and Richard S. Blumberg[1,*]
[1]Division of Gastroenterology, Department of Medicine
[2]Department of Pathology
Brigham and Women's Hospital, Harvard Medical School, 75 Francis Street, Boston, MA 02115, USA
[3]Department of Immunology and Infectious Diseases, Harvard School of Public Health, 651 Huntington Avenue, Boston, MA 02115, USA
[4]Institute for Clinical Molecular Biology, Christian-Albrechts-University Kiel, Schittenhelmstrasse 12, D-24105 Kiel, Germany
[5]Christian-Doppler Research Laboratory for Gut Inflammation and Division of Gastroenterology and Hepatology, Department of Medicine, Innsbruck Medical University, Anichstrasse 35, 6020 Innsbruck, Austria
[6]Division of Pediatric Gastroenterology, Erasmus MC–Sophia Children's Hospital, Dr Molewaterplein 60 3000 GE Rotterdam, The Netherlands
[7]Department of Microbiology and Molecular Genetics
[8]Department of Medicine
Harvard Medical School, 200 Longwood Avenue, Boston, MA 02115, USA
[9]First Department of Medicine, University Hospital Schleswig-Holstein, Schittenhelmstrasse 12, D-24105 Kiel, Germany
[10]These authors contributed equally to this work
[11]Present address: Division of Gastroenterology, Department of Medicine, Innsbruck Medical University, Anichstrasse 35, 6020 Innsbruck, Austria
*Correspondence: lglimche@hsph.harvard.edu (L.H.G.), rblumberg@partners.org (R.S.B.)
DOI 10.1016/j.cell.2008.07.021

SUMMARY

Inflammatory bowel disease (IBD) has been attributed to aberrant mucosal immunity to the intestinal microbiota. The transcription factor XBP1, a key component of the endoplasmic reticulum (ER) stress response, is required for development and maintenance of secretory cells and linked to JNK activation. We hypothesized that a stressful environmental milieu in a rapidly proliferating tissue might instigate a proinflammatory response. We report that *Xbp1* deletion in intestinal epithelial cells (IECs) results in spontaneous enteritis and increased susceptibility to induced colitis secondary to both Paneth cell dysfunction and an epithelium that is overly reactive to inducers of IBD such as bacterial products (flagellin) and TNFα. An association of *XBP1* variants with both forms of human IBD (Crohn's disease and ulcerative colitis) was identified and replicated (*rs35873774*; p value 1.6×10^{-5}) with novel, private hypomorphic variants identified as susceptibility factors. Hence, intestinal inflammation can originate solely from XBP1 abnormalities in IECs, thus linking cell-specific ER stress to the induction of organ-specific inflammation.

INTRODUCTION

In eukaryotes, signals emanating from the endoplasmic reticulum (ER) induce a transcriptional program that enables cells to survive ER stress. This highly coordinated response, the unfolded protein response (UPR), facilitates the folding, processing, export, and degradation of proteins emanating from the ER during stressed conditions (Ron and Walter, 2007). Three distinct UPR signaling pathways exist in mammalian cells that include ER transmembrane inositol-requiring enzyme 1α and β (IRE1α and β), pancreatic ER kinase (PERK), and activating transcription factor 6 (ATF6) (Wu and Kaufman, 2006). The most evolutionarily conserved of these is the kinase/endoribonuclease IRE1, whose activation by ER stress results in the excision of a 26 bp fragment from the mRNA encoding the transcription factor X-box-binding protein 1 (XBP1) by an unconventional splicing event that generates XBP1s, a potent inducer of a subset of UPR target genes (Calfon et al., 2002). XBP1s is required for ER expansion (Shaffer et al., 2004), the development of highly secretory cells such as plasma cells and pancreatic and salivary gland epithelial cells, and adaptation of tumor cells to hypoxic conditions and glucose deprivation (Reimold et al., 2001; Lee et al., 2005). XBP1s directs transcription of a core group of genes involved in constitutive maintenance of ER function in all cell types, and a remarkably diverse set of tissue- and condition-specific targets (Acosta-Alvear et al., 2007; Lee et al., 2003b; Shaffer et al., 2004). Intestinal epithelial cells (IECs) additionally express IRE1β, whose deletion results in increased ER stress and exacerbated dextran sodium sulfate (DSS) -induced colitis (Bertolotti et al., 2001).

We hypothesized that a stressful environmental milieu in cells with high secretory activity might induce inflammation. If so, inducing ER stress in vivo by cell-specific *Xbp1* deletion might lead to organ-specific inflammation, providing a mechanistic explanation for the initiation of proinflammatory diseases. We

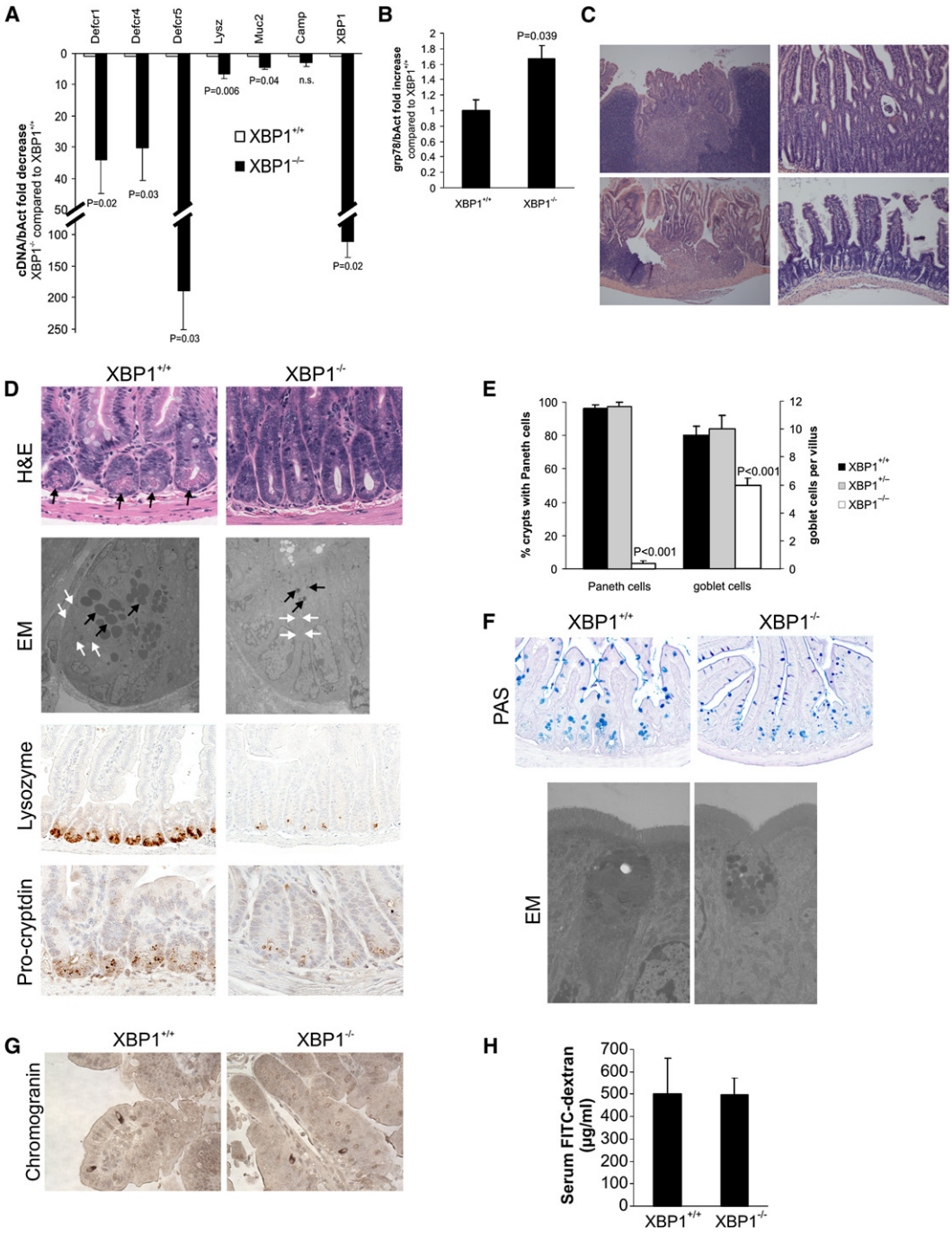

Figure 1. Spontaneous Enteritis and Paneth Cell Loss in *Xbp1*$^{-/-}$ Mice

(A) Small intestinal mucosal scrapings (n = 8 per group) from *Xbp1*-deleted (XBP1$^{-/-}$) and *Xbp1*-sufficient (XBP1$^{+/+}$) mouse intestinal epithelium were analyzed for cryptdin-1 (*Defcr1*), cryptdin-4 (*Defcr4*), cryptdin-5 (*Defcr5*), lysozyme (*Lysz*), mucin-2 (*Muc2*), cathelicidin (*Camp1*), and XBP1 (primers binding in the floxed region) mRNA expression. Data are expressed as fold decrease in *Xbp1*$^{-/-}$ compared to *Xbp1*$^{+/+}$ specimens, normalized to β-actin (mean ± SEM, Student's t test).

(B) Fold increase in grp78 mRNA expression in *Xbp1*$^{-/-}$ compared to *Xbp1*$^{+/+}$ epithelium, normalized to β-actin (n = 3 per group, mean ± SEM, Student's t test).

(C) Spontaneous enteritis in *Xbp1*$^{-/-}$ mice (upper panels and lower left panel), and normal histology of *Xbp1*$^{+/+}$ mice (lower right panel). Upper left, cryptitis with villous shortening, crypt regeneration, and architectural distortion; upper right, neutrophilic crypt abscesses; lower left, duodenitis with surface ulceration and granulation tissue.

(D) Paneth cells with typical eosinophilic granules on H&E-stained sections at the base of crypts in *Xbp1*$^{+/+}$, but not *Xbp1*$^{-/-}$, epithelium. Electron microscopy (EM) with only rudimentary electron-dense granules (black arrows) and a contracted ER (white arrows) in *Xbp1*$^{-/-}$ basal crypt epithelial cells, normal configuration in *Xbp1*$^{+/+}$ mice. Immunohistochemistry (IHC) for the granule proteins lysozyme and procryptdin in *Xbp1*$^{+/+}$ and *Xbp1*$^{-/-}$ epithelia.

focused on intestinal epithelium, which contains four highly secretory epithelial cell lineages that are exposed to high concentrations of exogenous antigens: absorptive epithelium, goblet, Paneth, and enteroendocrine cells that are derived from a common, constantly renewing intestinal epithelial stem cell (Barker et al., 2007). We show that induction of ER stress in intestinal epithelium through tissue- (and cell type-) specific disruption of *Xbp1* results in spontaneous enteritis due to inability of *Xbp1*-deficient IECs to properly generate antimicrobial activity and respond appropriately to inflammatory signals in the local milieu. Several single-nucleotide polymorphisms (SNPs) within the *XBP1* gene locus on chromosome *22q12.1* confer risk for both types of inflammatory bowel disease (IBD), Crohn's disease (CD) and ulcerative colitis (UC), establishing the ER stress pathway as a common genetic contributor to IBD in the human population. We provide herein a comprehensive in vivo framework for the manner in which hypomorphic variants of a novel IBD-susceptibility gene (*XBP1*) links ER stress within the epithelium to spontaneous intestinal inflammation.

RESULTS

Xbp1 Deletion in IEC Leads to ER Stress and Spontaneous Enteritis

$Xbp1^{flox/flox}$ mice were generated by targeting *loxP* sites to introns flanking exon 2, and bred onto Villin (V) -*Cre* transgenic mice (see Figures S1A–S1C available online), that directs *Cre* recombinase activity specifically to small and large intestinal epithelium (Madison et al., 2002). $Xbp1^{flox/flox}$*VCre* ($Xbp1^{-/-}$) offspring were born at a Mendelian ratio and developed normally. *Xbp1* exon 2 was efficiently and functionally deleted specifically within the intestinal epithelium (99% in small intestine, 87 ± 4% in colon) (Figures 1A, S1D, and S1E). Elevated basal grp78 levels in $Xbp1^{-/-}$ small intestinal epithelia indicated increased ER stress (Figure 1B) that was confirmed by microarray analysis showing both increased grp78 (*Haspa5*) and Chop (*Ddit3*) (P = 0.02) (Table S1; Figure S2A). Spontaneous small intestinal mucosal inflammation, in association with increased ER stress, occurred in 19/31 (61%) adult $Xbp1^{-/-}$ but not in (0/20) $Xbp1^{+/+}$ mice (χ^2 $P = 9.87 \times 10^{-6}$; Figure 1C). Notably, 5/16 (31%) heterozygous $Xbp1^{flox/wt}$*VCre* "$Xbp1^{+/-}$" mice displayed mild spontaneous small intestinal inflammation (χ^2 P = 0.007; Figure S2B). The inflammatory changes were patchy and ranged in severity from lamina propria polymorphonuclear infiltrates to crypt abscesses and frank ulcerations without granulomas (Figures 1C and S2B).

Absent Paneth Cells and Reduced Goblet Cells in $Xbp1^{-/-}$ Epithelium

$Xbp1^{-/-}$ intestine was completely devoid of Paneth cells (Figures 1D and 1E), compared to $Xbp1^{+/+}$ and $Xbp1^{+/-}$ mice (Figures 1E and S2B). Paneth cell granules store lysozyme and proforms of cryptdins, which were barely detectable in $Xbp1^{-/-}$ crypts (Figure 1D), and electron microscopy (EM) confirmed few rudimentary electron-dense granules of minute size and a compressed ER in $Xbp1^{-/-}$ Paneth cells (Figure 1D). mRNA expression of cryptdins-1, -4, and -5 and lysozyme, but not cathelicidin, were substantially reduced (Figure 1A). We also noted reduced numbers and size of goblet cells within the small intestine but not colon with reduced secretory granules by EM and reduced mRNA for the goblet cell protein MUC2 in $Xbp1^{-/-}$ small intestinal epithelia (Figures 1A, 1E, 1F, and S2C). Enteroendocrine cells were unaffected (Figures 1G and S2D) and the epithelial barrier function of absorptive epithelia was normal (Figure 1H). Thus, $Xbp1^{-/-}$ mice exhibited a major defect in Paneth cells and a minor defect in goblet cells in the small intestine with an unperturbed epithelial barrier.

Xbp1 Deletion Results in Apoptosis of Differentiated Paneth Cells and Exhibits Signs of a Regenerative Response

Quantitative PCR (qPCR; β-catenin, Tcf4, Math1, Hes1; Figure S3A), microarray analysis (Table S1), and β-catenin distribution (Figure S3B) of $Xbp1^{-/-}$ and $Xbp1^{+/+}$ intestinal epithelium did not reveal significant alterations in factors involved in intestinal epithelial cell fate decisions (Barker et al., 2007). We hypothesized that the highly secretory Paneth cell might undergo programmed cell death from failure to manage ER stress as observed in pancreatic acinar cells (Lee et al., 2005). Indeed, a few pyknotic, apoptotic cells were detected in $Xbp1^{-/-}$ crypts (antiactive caspase-3^+ and $TUNEL^+$; Figures 2A and S4A). To circumvent the problems associated with detecting a low-frequency event (apoptosis) in a slowly replenishing cell population, we generated $Xbp1^{floxneo/floxneo}$Villin-*Cre-ER*^{T2} mice (Figure S1A). Along with efficient deletion of *Xbp1* after initiation of tamoxifen treatment (Figure 2B), Paneth cell numbers were reduced by 98% on day 7, paralleled by a similar decrease in cryptdin-5 mRNA transcripts. Apoptotic epithelial nuclei (Figures 2C and S4B) were observed after 2.7 days, peaked at day 5, and declined on day 7 (Figure 2D). Apoptotic cells were present at the base of crypts (Paneth cells), and in villous epithelium (goblet cells) (Figure 2C). We observed a gradual increase of TNFα and Chop (*Ddit3*) mRNA (Figures 2B and 2E), similar to $Xbp1^{-/-}$ mice (Table S1; Figure S2A). We noted small intestinal inflammation in individual $Xbp1^{floxneo/floxneo}$Villin*Cre-ER*^{T2} mice at all time points analyzed (2.7, 5, and 7 days); focal enteritis was present in 4 of 9 mice at day 5 (44%) ranging from lamina propria polymorphonuclear infiltrates to crypt abscesses and frank ulcerations (Figure 2F, upper two panels), despite only minor reductions in Paneth cells (Figure 2F, lower panel). Cumulatively, at all time points examined, we observed enteritis in 7/18 (39%) $Xbp1^{floxneo/floxneo}$Villin*Cre-ER*^{T2} and 0/7 controls after induction with tamoxifen. The small intestinal epithelium exhibited villus shortening with a reduction of the villus:crypt ratio (Figure 2G), indicative of a regenerative response in $Xbp1^{-/-}$ mice. A 1 hr pulse of bromodeoxyuridine (BrdU) labeled the proliferative pool of

(E) Enumeration of Paneth cells and goblet cells in small intestines (n = 5 per group, mean ± SEM, Student's t test).
(F) Goblet cell staining by periodic acid Schiff (PAS) stain in $Xbp1^{+/+}$ and $Xbp1^{-/-}$ epithelia. EM exhibited smaller cytoplasmic mucin droplets and a contracted ER in $Xbp1^{-/-}$ goblet cells. No structural abnormalities were found in neighboring absorptive epithelia in $Xbp1^{-/-}$ mice.
(G) The marker for enteroendocrine cells, chromogranin, was detected by IHC in small intestines of $Xbp1^{+/+}$ and $Xbp1^{-/-}$ mice.
(H) $Xbp1^{+/+}$ and $Xbp1^{-/-}$ mice were orally administered FITC-dextran, and FITC-dextran serum levels were assayed 4 hr later (n = 7 per group, mean ± SEM).

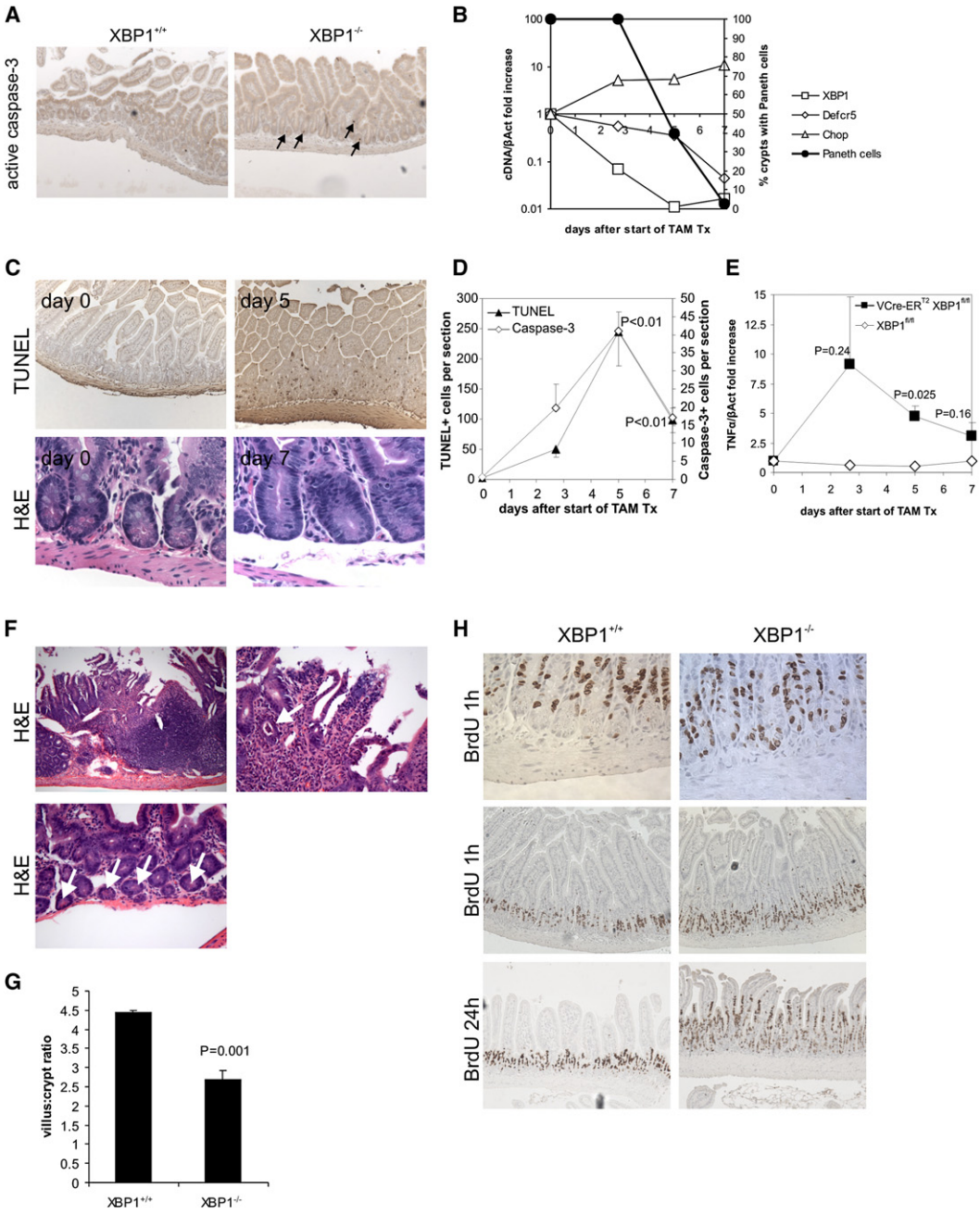

Figure 2. *Xbp1* Deletion Results in Apoptotic Paneth Cell Loss, Inflammation, a Distorted Villus:Crypt Ratio, and IEC Hyperproliferation

(A) Apoptotic nuclei were identified in *Xbp1*$^{-/-}$ (*Xbp1*$^{flox/flox}$*VCre*) and *Xbp1*$^{+/+}$ (*Xbp1*$^{flox/flox}$) sections with antiactive (cleaved) caspase-3. Arrows point to apoptotic cells.

(B) *Xbp1*$^{floxneo/floxneo}$*VCre-ER*^{T2} mice were administered five daily intraperitoneal doses of 1 mg tamoxifen to induce deletion of the *Xbp1*^{floxneo} gene in the intestinal epithelium. XBP1, cryptdin-5 (*Defcr5*), and Chop mRNA (all expressed normalized to β-actin; left y axis) expression in epithelium during and after tamoxifen treatment. Percentage of crypts with Paneth cells on H&E staining is shown (right y axis). Representative experiment of three performed.

(C) TUNEL and H&E staining on small intestinal sections of tamoxifen-treated *Xbp1*$^{floxneo/floxneo}$*VCre-ER*^{T2} mice collected at the indicated days.

(D) TUNEL^{+} and caspase-3^{+} cells were enumerated by light microscopy (three mice per time point with ileal and jejunal sections each; mean ± SEM; p values indicate comparisons to time point 0; Student's t test).

(E) TNFα mRNA was quantified by qPCR in small intestinal epithelial scrapings from ileum harvested at the indicated time points after start of tamoxifen administration from V*Cre-ER*^{T2} *Xbp1*$^{floxneo/floxneo}$ (n = 4 per time point) or *Xbp1*$^{floxneo/floxneo}$ (n = 1 per time point) mice. Mean ± SEM; p values indicate comparisons to time point 0; Student's t test.

(F) Enteritis in the small intestine in V*Cre-ER*^{T2} *Xbp1*$^{floxneo/floxneo}$ mice on day 5 after tamoxifen administration. Upper left panel, 100×; upper right panel, same section, 400×, arrow points to a crypt abscess; lower panel 100×, crypts with Paneth cells (arrows).

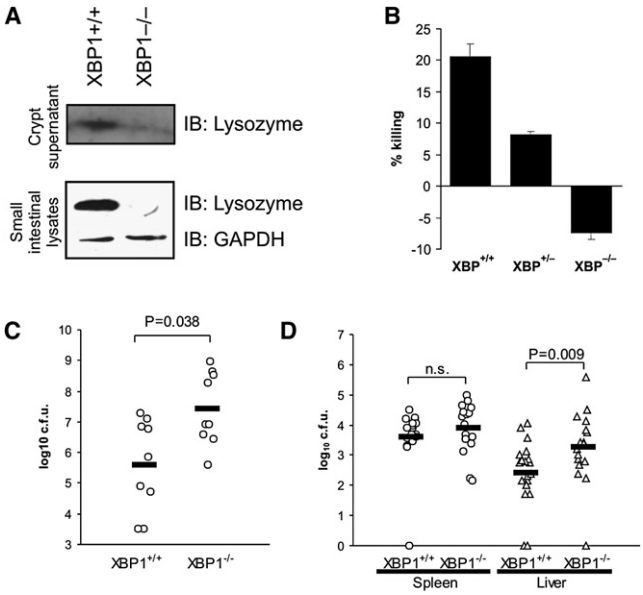

Figure 3. XBP1 Deficiency in Epithelium Results in Impaired Antimicrobial Function

(A) Lower panel: small intestinal tissue from *Xbp1*$^{+/+}$ and *Xbp1*$^{-/-}$ mice was homogenized, resolved on SDS-PAGE, and detected by anti-lysozyme IgG and GAPDH to ensure equal loading. Upper panel: small intestinal crypts isolated from *Xbp1*$^{+/+}$ and *Xbp1*$^{-/-}$ animals were stimulated with 10 μM carbamyl choline (CCh). Supernatants were precipitated, resolved on SDS-PAGE, and detected by anti-lysozyme IgG. Blots are representative of two independent experiments.

(B) Small intestinal crypts were stimulated with LPS for 30 min, and supernatants were assayed for bactericidal activity. Data are expressed as % killing compared to unstimulated crypts (triplicates, mean ± SEM), and are representative of two independent experiments.

(C) Intestinal epithelial cell-specific *Xbp1*$^{-/-}$ mice (n = 9) and *Xbp1*$^{+/+}$ littermates (n = 9; 5–10 weeks of age) were perorally infected with 3.6 × 10^{8} *L. monocytogenes*. Feces was aseptically collected 10 hr after infection and colony forming units (c.f.u.) of *L. monocytogenes* were determined. Data are presented as c.f.u. per mg dry weight of feces.

(D) Oral infection with *L. monocytogenes* was performed as in (C), liver and spleen were aseptically harvested 72 hr after infection, and c.f.u. of *L. monocytogenes* were determined (*Xbp1*$^{+/+}$, n = 20; *Xbp1*$^{-/-}$, n = 17). Data are expressed as c.f.u. per organ. A two-tailed Mann-Whitney test was performed for (C) and (D).

intestinal stem cells, and was similar in *Xbp1*$^{+/+}$ and *Xbp1*$^{-/-}$ mice (Figure 2H). However, 24 hr after BrdU injection, labeled cells were detected higher up in the crypt-villus axis in *Xbp1*$^{-/-}$ mice, indicating an increased migration rate (Figure 2H). Thus, XBP1 affects IEC homeostasis both through controlling cell renewal and cell death.

Xbp1 Deletion Impairs Mucosal Defense to Oral *Listeria monocytogenes* Infection

Xbp1$^{-/-}$ small intestinal lysates and supernatants lacked detectable lysozyme in response to carbamyl choline (CCh) (Figure 3A) or lipopolysaccharide (LPS) (not shown), and LPS-elicited *Xbp1*$^{-/-}$ crypt supernatants lacked bactericidal killing activity (Figure 3B). Oral infection with *Listeria monocytogenes*, a Gram-positive intracellular pathogen that is affected by Paneth cell defects (Kobayashi et al., 2005), revealed that 10 hr after infection, 100-fold higher numbers of colony forming units (c.f.u.) of *L. monocytogenes* were recoverable from feces of *Xbp1*$^{-/-}$ compared to *Xbp1*$^{+/+}$ mice (Figure 3C). Translocation into liver and spleen after 72 hr revealed a 10-fold higher number of *L. monocytogenes* recovered from *Xbp1*$^{-/-}$ livers, but similar numbers from spleen (Figure 3D). These data suggest that XBP1 in Paneth cells is required to decrease the luminal burden of *L. monocytogenes*.

XBP1 Deficiency Results in Enhanced Responses of IECs to Typical Mucosal Inflammatory Signals

XBP1 mRNA splicing is a marker of IRE1 activation and ER stress (Calfon et al., 2002; Lin et al., 2007). Virtually complete splicing of mutant XBP1 mRNAs in *Xbp1*$^{-/-}$ small and large intestine and partial splicing in *Xbp1*$^{+/-}$ small intestine was observed in contrast to barely detectable splicing in *Xbp1*$^{+/+}$ mice (Figure 4A), indicating IRE1 hyperactivation. JNK phosphorylation was increased in *Xbp1*$^{-/-}$ small intestinal epithelia compared to controls, consistent with the described TRAF2-dependent function of IRE1 to activate JNK (Urano et al., 2000) (Figure 4B). To test whether XBP1-mediated intestinal inflammation arose from increased JNK activity in a microbiota- and cytokine-free system, we silenced XBP1 expression in the mouse IEC line MODE-K with an siRNA retrovirus (iXBP) and used flagellin and TNFα as proinflammatory stimulants (Lodes et al., 2004). TNFα and flagellin increased JNK phosphorylation and CXCL1 production from MODE-K.iXBP (50%–90% reduction of XBP1) compared to MODE-K.Ctrl cells (Figures 4C–4E) that was dose-dependently and specifically (Figures S5A and S5B) blocked by the JNK inhibitor SP600125 (Figures 4F and 4G), but did not affect CD1d-restricted MODE-K antigen presenting function (van de Wal et al., 2003) (Figure 4H). We conclude that impaired XBP1 expression directly heightens proinflammatory JNK/SAPK signaling in IECs in response to environmental stimuli and may contribute to Paneth, goblet cell, and MODE-K.iXBP apoptosis (Figures 2A, 2C, 2D, S6A, and S6B).

XBP1 Deficiency Leads to Increased Susceptibility to Experimental Colitis

The *Xbp1*$^{-/-}$ colon, unlike the small intestine, did not exhibit spontaneous colitis, but colonic IECs displayed evidence of increased ER stress (Figure 4A). We therefore examined the in vivo effects of DSS, a toxin for mucosal epithelial cells that disrupts barrier function (Strober et al., 2002). *Xbp1*$^{-/-}$ mice given 4.5% DSS in drinking water exhibited more severe wasting and rectal bleeding than *Xbp1*$^{+/+}$ littermates (Figures 5A and 5B). Histologically, *Xbp1*$^{-/-}$ colons displayed increased areas of mucosal erosions, edema, and cellular infiltration along with increased

(G) Jejunal sections of *Xbp1*$^{flox/flox}$ (*Xbp1*$^{+/+}$; n = 7) and *Xbp1*$^{flox/flox}$*VCre* (*Xbp1*$^{-/-}$; n = 8) mice were assessed for their villus:crypt ratio on H&E stainings (ratios of ≥4:1 are considered normal for jejunum; mean ± SEM, Student's t test).

(H) *Xbp1*$^{flox/flox}$ (*Xbp1*$^{+/+}$) and *Xbp1*$^{flox/flox}$*VCre* (*Xbp1*$^{-/-}$) mice were administered bromodeoxyuridine (BrdU) intraperitoneally, and small intestinal sections were harvested after 1 and 24 hr (n = 3 per genotype per time point). The 1 hr time point labels the pool of proliferating IECs in the crypts (mostly transit amplifying IEC), whereas the 24 hr time point assesses the migration along the crypt-villus axis indicating the turnover of the IEC compartment.

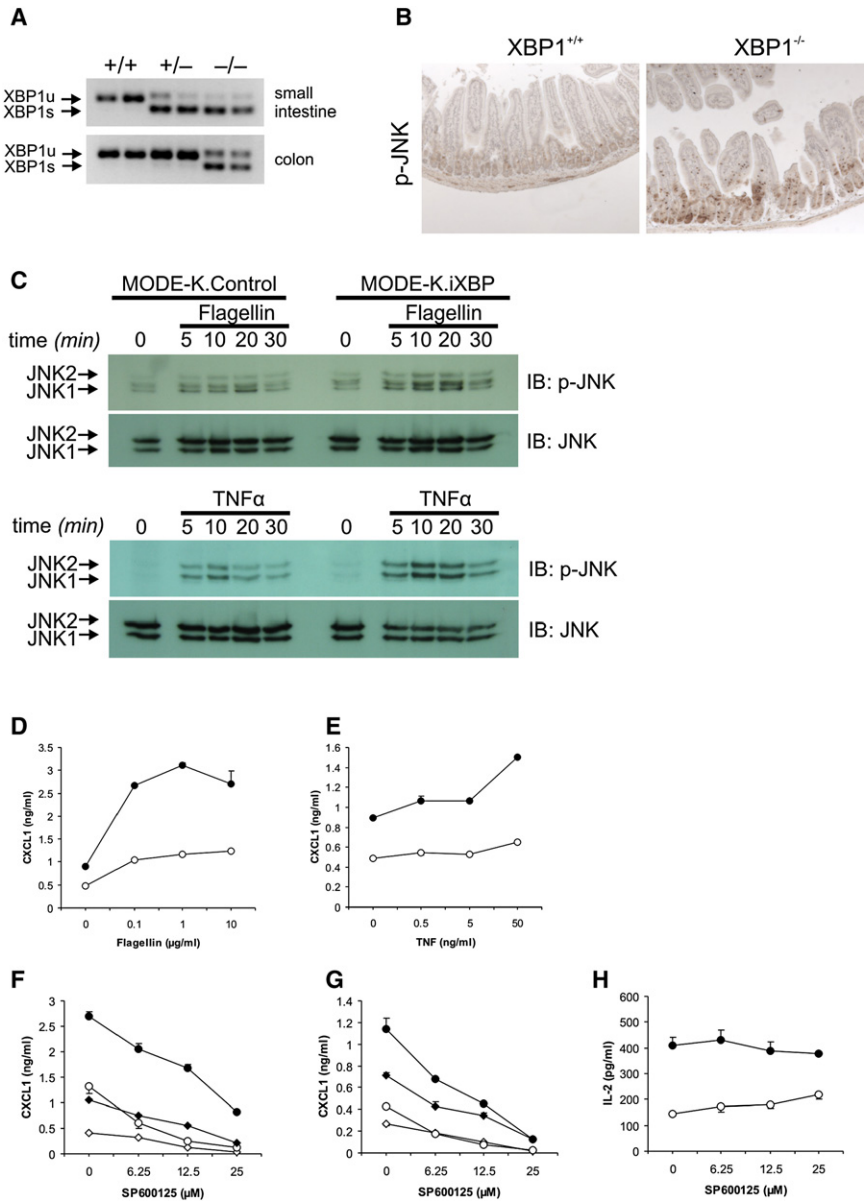

Figure 4. XBP1 Deficiency Results in Increased Inflammatory Tone of the Epithelium

(A) Small intestinal and colonic epithelial mRNA scrapings from *Xbp1*$^{+/+}$, *Xbp1*$^{+/-}$, and *Xbp1*$^{-/-}$ mice were analyzed for XBP1 mRNA splicing status.

(B) Small intestinal formalin-fixed sections were stained with rabbit anti-phospho-JNK antibody, and revealed a patchy staining pattern in *Xbp1*$^{-/-}$, but not *Xbp1*$^{+/+}$, sections. Control rabbit mAb was negative (not shown). Representative of n = 5 per group.

(C) MODE-K.iXBP and MODE-K.Control were stimulated for the indicated time periods with flagellin (1 μg/ml) and TNFα (50 ng/ml) and analyzed for P-JNK and total JNK by western blot.

(D) MODE-K.iXBP (filled circles) and MODE-K.Ctrl (open circles) cells were stimulated for 4 hr with flagellin, and supernatants were assayed by ELISA for CXCL1. Triplicates, mean ± SEM.

(E) Experiment as in (D), with TNFα.

(F) MODE-K.iXBP (circles) and MODE-K.Ctrl (diamonds) cells were stimulated with either 10 μg/ml flagellin (filled symbols) or media alone (open symbols) for 4 hr with the JNK inhibitor SP600125, and supernatants were assayed for CXCL1. Triplicates, mean ± SEM.

(G) As in (F), MODE-K cells were stimulated with 50 ng/ml TNFα (filled symbols) or media alone (open symbols).

(H) MODE-K.iXBP (filled circles) and MODE-K.Ctrl (open circles) cells were loaded with the glycolipid antigen α-galactosylceramide (αGC), fixed, and cocultured with the CD1d-restricted NKT cell hybridoma DN32.D3, and antigen presentation was measured as IL-2 release from DN32.D3. Triplicates, mean ± SEM.

crypt loss compared to *Xbp1*$^{+/+}$ littermates (Figures 5C and 5D). *Xbp1*$^{+/-}$ mice exhibited an intermediate phenotype (Figures 5A–5C). Antibiotic treatment abrogated the differences in severity of DSS colitis between *Xbp1*$^{+/+}$ and *Xbp1*$^{-/-}$ mice (Figures S7A and S7B), highlighting the importance of the commensal flora in the colitis observed (Figures 5A–5D). Levels of TNFα, a central mediator of inflammation in DSS colitis (Kojouharoff et al., 1997), were elevated in DSS-treated *Xbp1*$^{-/-}$ versus *Xbp1*$^{+/+}$ colonic tissues with intermediate TNFα expression in *Xbp1*$^{+/-}$ mice (Figure 5E).

Human Ileal and Colonic Mucosa in CD and UC Exhibit Signs of ER Stress

We analyzed UPR activation in the intestine of healthy individuals and CD and UC patients in ileal and colonic biopsies. grp78 expression was increased in inflamed ileal CD mucosa and XBP1s levels were increased in both inflamed and noninflamed ileal CD biopsies (Figure 5F). Similarly, XBP1s levels in inflamed and noninflamed colonic CD and UC mucosa were increased compared to those from healthy individuals, and there was a trend toward increased grp78 expression in inflamed UC and CD specimens (Figure 5G). These data indicate the presence of ER stress and increased IRE1 activity in the ileum and colon of CD and UC patients.

SNPs within the *XBP1* Gene Region Are Associated with IBD

Three previously reported genome-wide linkage studies independently suggested linkage of the *22q12* region with IBD (Hampe et al., 1999; Barmada et al., 2004; Vermeire et al., 2004), with signals as close as 0.3 Mb from the *XBP1* gene. We examined a German patient cohort of 1103 controls and 550 CD and 539 UC patients (panel 1), genotyping for 20 tagging SNPs (average SNP distance, 5.25 kb; Figures S8A–S8E),

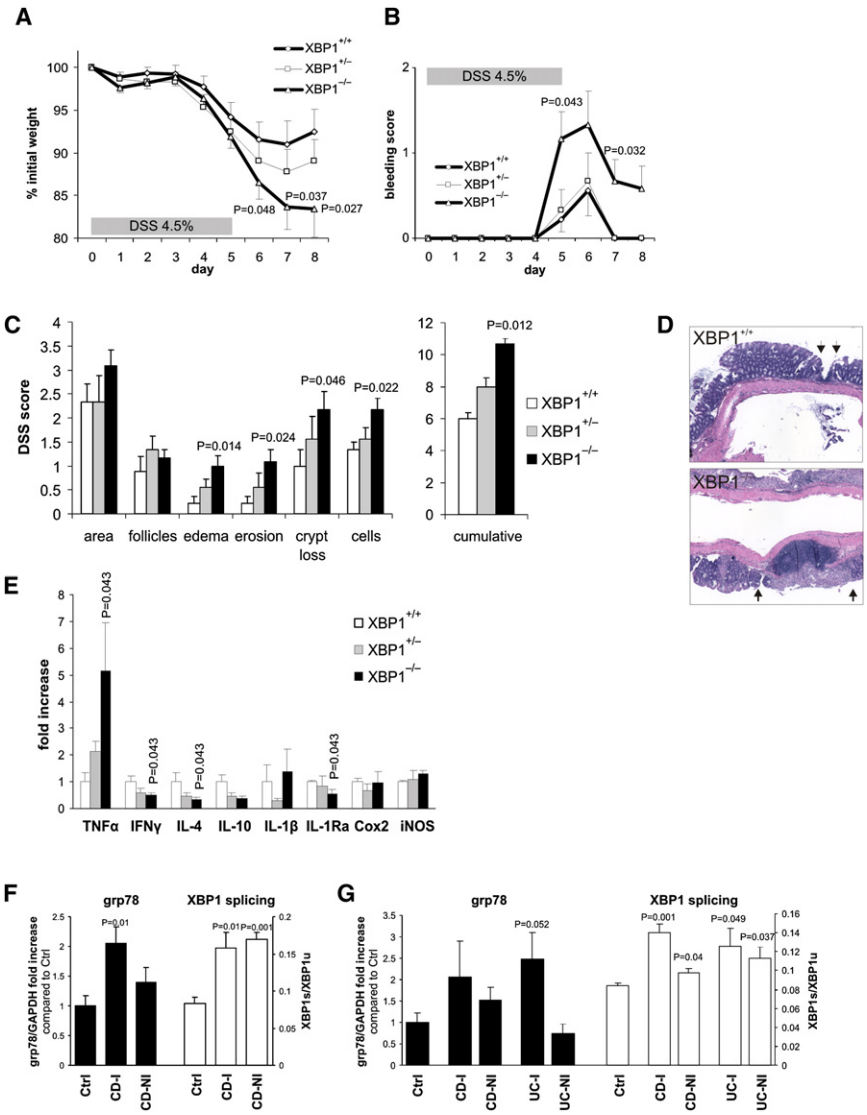

Figure 5. XBP1 Deficiency Increases Susceptibility to DSS Colitis

(A) DSS (4.5%) was administered in drinking water for 5 days and then replaced by regular drinking water in *Xbp1*$^{+/+}$ (n = 9), *Xbp1*$^{+/-}$ (n = 9), and *Xbp1*$^{-/-}$ (n = 12) littermates (age 6–12 weeks). Wasting is presented as % of initial weight, mean ± SEM. A one-tailed Student's t test was performed.

(B) Presence of rectal bleeding during DSS colitis was assessed daily and scored as in Experimental Procedures. Mean ± SEM; *Xbp1*$^{+/+}$ (n = 9), *Xbp1*$^{+/-}$ (n = 9), *Xbp1*$^{-/-}$ (n = 12). A two-tailed Mann-Whitney test was performed.

(C) Individual signs of inflammation of colonic tissue harvested on day 8 of DSS colitis were scored blindly. A two-tailed Mann-Whitney test was performed, mean ± SEM.

(D) Typical colonic histology on day 8 of DSS colitis. Arrows indicate borders of ulcers.

(E) mRNA expression (normalized to β-actin) of inflammatory mediators was quantified by qPCR in colonic specimens on day 8 of DSS colitis. n = 4 per group. Mean ± SEM was analyzed by a two-tailed Mann-Whitney test.

(F) Human ileum in Crohn's disease exhibits signs of ER stress. Inflamed (CD-I; n = 3) and noninflamed (CD-NI; n = 3) ileal biopsies from CD patients and healthy control (Ctrl; n = 4) subjects were analyzed for grp78 mRNA expression (levels in controls were arbitrarily set at 1, and CD-I and CD-NI levels are expressed as ratio to controls; left y axis). XBP1 mRNA splicing is expressed as the ratio of XBP1s:XBP1u (right y axis). Mean ± SEM.

(G) Human colon mucosa in Crohn's disease (CD) and ulcerative colitis (UC) exhibits signs of ER stress. Colonic biopsies from inflamed (-I) and noninflamed (-NI) CD and UC patients (n = 3 each) and healthy control subjects (Ctrl; n = 4) were analyzed for grp78 mRNA expression and XBP1 splicing as described in (F).

selected from HapMap data of individuals of European ancestry using de Bakker's algorithm as implemented in Haploview (Barrett et al., 2005). Three SNPs were significantly associated with IBD: *rs5997391*, *rs5762795*, and *rs35873774* (Table 1). The last SNP, located in intron 4/5 of *XBP1*, remained significantly associated after correcting for multiple testing using Bonferroni correction (p value = 0.0011).

We replicated this index finding by genotyping two additional independent patient panels (panel 2: 1854 patients, 2042 controls; panel 3: 1446 patients, 2177 controls) and reproduced the significant association with two of these three index SNPs in each panel (*rs5997391* and *rs5762795* in panel 2; *rs5762795* and *rs35873774* in panel 3; Table 1; Table S2). Significant associations of nine and six additional SNPs in panels 2 and 3, respectively, with CD, UC, and/or IBD were obtained. Several association signals in each panel were robust to correction for multiple testing and remained significant after 10,000 permutations. The combined analysis of panels 1, 2, and 3 in a total of 5322 controls and 2762 CD and 1627 UC patients identified a total of six SNPs associated with IBD that were robust after correction for multiple testing and significant after 10,000 permutations; the minor alleles of these six SNPs conferred protection from IBD (Table 1; Figure S8A). The strongest associated variant was *rs35873774* (p value = 1.6×10^{-5}). The odds ratio (OR) for carriership of the rarer C allele of *rs35873774* in the combined IBD panel was 0.74 (95% confidence interval [CI], 0.66–0.84; Table 1).

Among the 20 SNPs tested, markers 2–5, 7, 9–14, and 18–20 (Table 1) are located in a 99 kb large block. Table S3 summarizes the haplotype analysis results of the seven-marker haplotype tagging SNPs of this block (2–4, 9–10, 12, 18). Three of the eight haplotypes were significantly associated with IBD after 10,000 permutations. Haplotypes 5 and 7 were protective, whereas 4 was a risk haplotype. Multiple logistic regression analysis of the entire IBD panel including gender as a covariate revealed a best-model fit with SNPs *rs5997391* and *rs35873774* (intron 4/5 of

Table 1. Association Results of 20 SNPs that Were Genotyped across the *XBP1* Gene Region

					Panel 1 (1103 Controls, 550 CD, 539 UC)						Panel 2 (2042 Controls, 1303 CD, 551 UC)						Panel 3 (2177 Controls, 909 CD, 537 UC)						Panel 1 + 2 + 3 (5322 controls, 2762 CD, 1627 UC)	
#	dbSNP ID	Position	Distance (kb)	A1	MAF U	MAF CD	MAF UC	p Value CD	p Value UC	p Value IBD	MAF U	MAF CD	MAF UC	p Value CD	p Value UC	p Value IBD	MAF U	MAF CD	MAF UC	p Value CD	p Value UC	P Value IBD	P Value IBD	OR (95% CI) IBD
1	rs714191	27,469,965	-	C	0.18	0.19	0.18	0.45	0.79	0.53	0.18	0.18	0.18	0.39	0.84	0.45	0.18	0.20	0.19	0.078	0.48	0.097	0.086	1.07 (0.98–1.16)
2	rs5997391[a]	27,470,093	0.13	T	0.07	0.06	0.05	0.15	**0.012**	**0.014**	0.06	0.05	0.05	0.057	**0.036**	**0.014**	0.07	0.06	0.06	0.15	0.12	0.058	**0.000072**[b,c]	0.79 (0.69–0.89)
3	rs5752792[a]	27,478,313	8.22	C	0.16	0.17	0.18	0.50	0.085	0.15	0.17	0.18	0.19	0.45	0.099	0.19	0.18	0.19	0.18	0.21	0.58	0.22	**0.031**	1.08 (0.99–1.18)
4	rs6005863[a]	27,481,002	2.69	G	0.41	0.41	0.39	0.84	0.25	0.41	0.41	0.40	0.37	0.43	**0.032**	0.12	0.42	0.44	0.39	0.07	0.11	0.62	0.22	0.98 (0.90–1.07)
5	rs5762788	27,499,324	18.32	A	0.33	0.30	0.31	0.10	0.44	0.12	0.32	0.29	0.28	**0.0032**	**0.024**	**0.00081**[b,c]	0.32	0.33	0.28	0.70	**0.012**	0.30	**0.00042**[b,c]	0.85 (0.78–0.92)
6	rs6005879	27,502,868	3.54	A	0.05	0.04	0.05	0.17	0.94	0.39	0.05	0.04	0.05	**0.016**	0.52	**0.032**	0.05	0.05	0.05	0.45	0.55	0.39	0.22	0.92 (0.80–1.06)
7	rs5752797	27,504,552	1.68	T	0.17	0.18	0.17	0.85	0.83	0.98	0.18	0.16	0.16	0.11	0.18	0.065	0.18	0.21	0.17	**0.00089**[b,c]	0.70	**0.025**	0.86	1.00 (0.91–1.09)
8	rs5997403	27,505,938	1.39	T	0.05	0.04	0.05	0.25	0.99	0.48	0.04	0.04	0.04	0.091	0.76	0.15	0.04	0.04	0.05	0.79	0.53	0.60	0.34	0.94 (0.81–1.09)
9	rs5762795[a]	27,507,054	1.12	A	0.33	0.30	0.30	0.10	0.084	**0.039**	0.32	0.29	0.28	**0.0082**	**0.016**	**0.0016**[b,c]	0.32	0.33	0.28	0.73	**0.00469**[b]	0.22	**0.00012**[b,c]	0.84 (0.78–0.92)
10	rs2267131[a]	27,515,025	7.97	C	0.12	0.14	0.13	0.39	0.84	0.51	0.14	0.12	0.12	0.12	0.096	0.051	0.13	0.16	0.11	**0.00353**[b]	0.20	0.13	0.92	0.96 (0.87–1.05)
11	rs2097461	27,516,433	1.41	C	0.33	0.30	0.30	0.14	0.16	0.077	0.32	0.29	0.27	**0.012**	**0.0044**	**0.0013**[b,c]	0.32	0.33	0.28	0.67	**0.00573**[b]	0.25	**0.00023**[b,c]	0.85 (0.78–0.92)
12	rs35873774[a]	27,516,485	0.05	C	0.08	0.05	0.06	**0.0028**	**0.028**	**0.0011**[b,c]	0.07	0.07	0.06	0.82	0.30	0.53	0.08	0.05	0.05	**0.00342**[b]	**0.00147**[b,c]	**0.000092**[b,c]	**0.000016**[b,c]	0.74 (0.66–0.84)
13	rs2269578	27,521,397	4.91	C	0.12	0.13	0.13	0.71	0.52	0.54	0.13	0.12	0.11	0.10	0.089	**0.043**	0.13	0.15	0.12	**0.017**	0.27	0.24	0.76	0.94 (0.85–1.04)
14	rs3788409	27,522,705	1.31	G	0.33	0.30	0.31	0.12	0.39	0.11	0.32	0.30	0.28	**0.025**	**0.029**	**0.0065**	0.33	0.33	0.28	0.79	**0.00493**[b]	0.19	**0.00097**[b,c]	0.85 (0.78–0.92)
15	rs6005893	27,524,344	1.64	T	0.05	0.04	0.04	0.23	0.17	0.11	0.05	0.03	0.04	**0.043**	0.18	**0.028**	0.04	0.05	0.05	0.27	0.18	0.13	0.19	0.91 (0.79–1.06)
16	rs35679096	27,524,947	0.60	A	0.03	0.03	0.03	0.45	0.32	0.28	0.04	0.03	0.03	0.43	0.18	0.24	0.03	0.04	0.03	0.39	0.97	0.55	0.38	0.93 (0.78–1.10)
17	rs133440	27,535,932	10.99	C	0.04	0.04	0.03	0.44	0.19	0.21	0.05	0.05	0.03	0.96	0.099	0.54	0.05	0.04	0.06	0.40	0.060	0.68	0.47	0.97 (0.84–1.12)
18	rs5762839[a]	27,556,001	20.07	T	0.17	0.16	0.17	0.72	0.82	0.90	0.17	0.15	0.14	**0.0039**	**0.032**	**0.0011**[b,c]	0.17	0.19	0.15	0.092	0.100	0.70	0.055	0.88 (0.80–0.96)
19	rs5762852	27,567,027	11.03	C	0.17	0.18	0.17	0.59	0.65	0.54	0.17	0.16	0.15	0.14	0.11	0.064	0.17	0.19	0.15	0.13	0.090	0.81	0.46	0.94 (0.86–1.03)
20	rs5762853	27,569,785	2.76	G	0.24	0.24	0.24	0.94	0.73	0.80	0.24	0.22	0.22	**0.029**	0.11	**0.017**	0.24	0.27	0.23	0.050	0.48	0.28	0.25	0.94 (0.86–1.02)

Single-point association results for the three independent patient panels and the combined IBD (i.e., CD + UC) panel are shown. Intermarker distances are shown in kilobases (kb) and positions refer to NCBI's build 35. Minor allele frequencies (MAF) are listed for unaffected controls (U), Crohn's disease (CD), and ulcerative colitis (UC) patients. p values are shown for the standard χ^2 test with one degree of freedom, and p values < 0.05 are highlighted by bold type. Odds ratios (OR) including 95% confidence intervals (95% CI) are shown for carriership of the rarer allele A1, and p values < 0.05 are highlighted by bold type. For detailed genotype counts, see Table S2.

[a] SNPs included in the seven-marker haplotype analysis (Table S3).

[b] p values that were significant after 10,000 permutations.

[c] p values that were significant after correcting for multiple testing using Bonferroni correction (Bonferroni significance threshold: p value < 0.0025).

XBP1). Logistic regression analysis did not reveal any statistically significant interaction between any of the 20 genotyped SNPs in XBP1.

Deep Sequencing Reveals Multiple Rare Variants Including Two Hypomorphic Variants that Might Confer Risk

Linkage disequilibrium (LD) around the *XBP1* gene, flanked by two recombination hotspots (Figure S8B), is generally weak (Figure S8E). The complex haplotype structure of the locus (Table S3) suggested that multiple rare, private SNPs might contribute to its IBD association. We resequenced all exons, splice sites, and promoter regions in 282 unaffected controls and 282 CD and 282 UC patients, and exons and splice sites only in an additional 282 UC patients (Table S4; Figure S9). Apart from verifying 15 already annotated variants, 51 new polymorphisms were identified, among them 39 rare SNPs detected once in either the CD, UC, and/or control cohort. The discovery frequency for rare SNPs was 5, 16, and 18 for 282 controls and CD and UC patients, respectively. Sequencing of the coding region in another 282 UC patients yielded another three novel SNPs. Five novel nonsynonymous SNPs (nsSNPs; *XBP1snp8*, *XBP1snp17*, *XBP1snp22*, *XBP1snp29*, *XBP1snp30*) were discovered in the sequencing cohort of 1128 patients but not controls. Taqman genotyping revealed the actual frequencies of these five novel nsSNPs in panels 1 and 2. Notably, heterozygous individuals were only observed among the case groups for four of the five rare nsSNPs, whereas the fifth nsSNP (*XBP1snp22*) occurred at equal frequencies in all groups (Table S4; Figure S9). The novel nsSNPs were too rare to warrant formal statistical analysis.

The nsSNPs *XBP1snp8* (M139I) and *XBP1snp17* (A162P) present in IBD patients but not controls (Table S4) lead to amino acid changes in the XBP1 hinge region between the bZiP and transactivation domains. *XBP1snp17* in exon 4 is 10 bp upstream of the XBP1 mRNA splice site recognized by IRE1. We engineered the respective mutations into unspliced (h*XBP1u*) and spliced (h*XBP1s*) versions and transiently cotransfected MODE-K cells with wild-type or mutant *XBP1* plasmids and an UPRE-luciferase reporter construct (Lee et al., 2003b). h*XBP1u*.M139I and h*XBP1s*.M139I had diminished UPRE transactivating function compared to wild-type plasmids in untreated and tunicamycin- (Tm) treated MODE-K (Figures 6A and 6B). h*XBP1u*.A162P displayed impaired UPRE transactivation only in Tm-treated MODE-K cells (Figure 6A), whereas h*XBP1s*.A162P transactivation was unaltered (Figure 6B). To test the ability to induce XBP1s target genes, we reconstituted *Xbp1*$^{-/-}$ mouse embryonic fibroblasts (MEFs) (Iwakoshi et al., 2003) with either wild-type or mutant h*XBP1u-GFP* retroviral constructs, obtaining similar GFP fluorescence and comparable protein levels (Figures 6C and 6D). h*XBP1*.M139I induced less ERdj4 (*DNAJB9*) and EDEM (*EDEM1*) mRNA than h*XBP1* wild-type both at baseline and upon Tm treatment, whereas h*XBP1u*.A162P was hypomorphic only under conditions of ER stress (Figure 6E) as above (Figures 6A and 6B). h*XBP1*.P15L (*XBP1snp22*), the only rare nsSNP present at similar frequencies in IBD patients and controls, was not hypomorphic in these assays (Figures S10A and S10B).

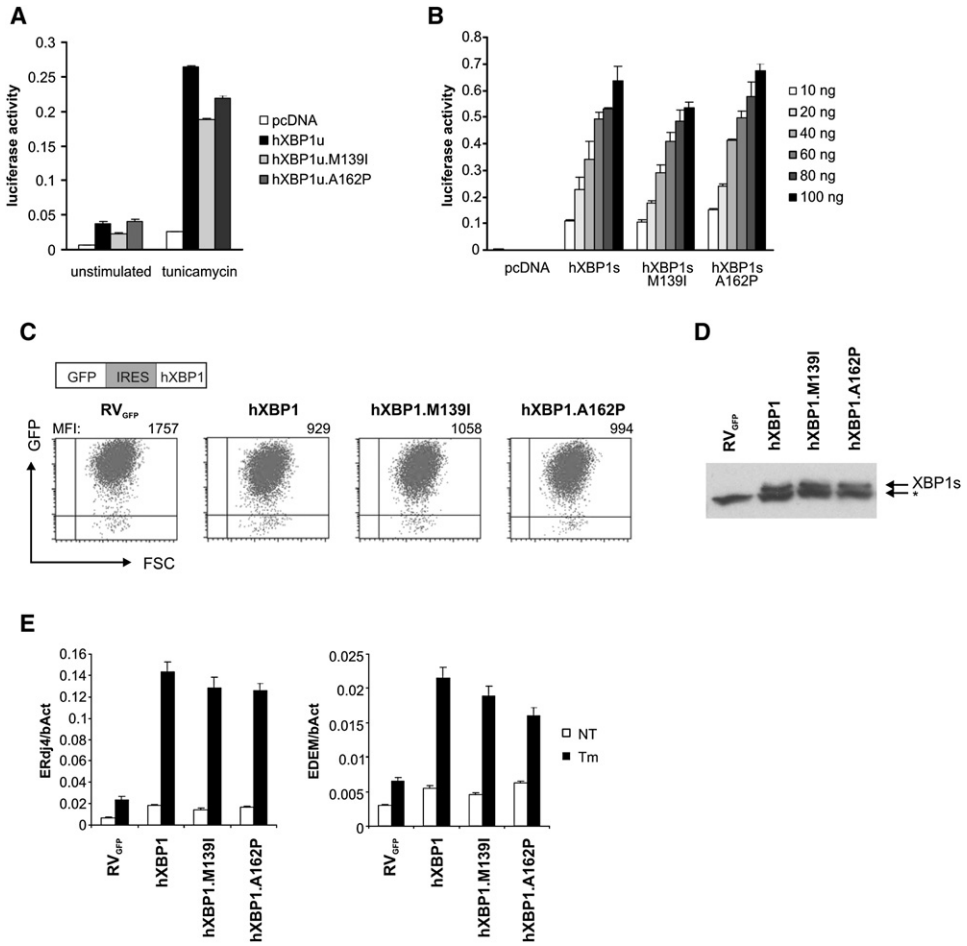

Figure 6. Rare *XBP1* Variants Are Hypomorphic

(A) MODE-K cells were transfected with UPRE-luciferase and unspliced hXBP1u expression plasmids encoding the rare, IBD-associated minor alleles *XBP1snp8* (M139I) and *XBP1snp17* (A162P) and treated with 1 μg/ml tunicamycin (Tm). Values represent luciferase activities normalized to cotransfected *Renilla* reporter. Duplicates, mean ± SD.

(B) Experiments as in (A), with indicated amounts of spliced hXBP1s cDNA variants.

(C) Transduction efficiency measured by fluorescence-activated cell sorting (FACS) of *Xbp1*$^{-/-}$ MEF cells reconstituted with human *XBP1* wild-type or SNP variants bicistronic retroviral vectors (RV_{GFP}) (MFI, mean fluorescence intensity; GFP, green fluorescent protein; FSC, forward scatter).

(D) XBP1s protein levels were determined by western blot of Tm-treated cells (*, nonspecific band).

(E) ERdj4 and EDEM mRNA levels (normalized to β-actin mRNA expression) in untreated (NT) or Tm- (1 μg/ml; 6 hr) treated *Xbp1*$^{-/-}$ MEF cells transduced with h*XBP1u-GFP* retroviral construct variants. Duplicates, mean ± SD.

DISCUSSION

We present a spontaneous mouse model of intestinal inflammation that arises from a gene defect in an actual genetic risk factor for human IBD. We suggest that XBP1 unifies key elements of IBD pathogenesis within the IEC compartment, pointing toward a primary defect in IEC function in IBD pathogenesis. Our results introduce the ER stress response as a likely integral component of organ-specific inflammation. XBP1 controls organ-specific inflammation through two major mechanisms that are probably codependent. First, Paneth cell function was strikingly impaired in *Xbp1*$^{-/-}$ mice, as evidenced by diminished antimicrobial peptide secretion and a compromised response to pathogenic bacteria. Second, XBP1 deficiency itself induced ER stress that led to a heightened proinflammatory response of the epithelium to known IBD inducers flagellin and TNFα (Figure S11).

XBP1 and Environmental Factors

Consistent with our results, increased grp78 expression has recently been reported in IBD patients (Shkoda et al., 2007; Heazlewood et al., 2008). Whereas Shkoda et al. suggested that ER stress occurs secondary to an inflammatory insult to IECs, our data instead point to specific impairment of the ER stress response as a cause, rather than a consequence, of intestinal inflammation. This might be obvious in the context of the genetic association of *XBP1* variants with IBD reported here, but we speculate that environmental factors may also impair XBP1 function (and hence the ER stress response). Monozygotic twin

studies have highlighted the importance of as yet unknown environmental and/or epigenetic factors in the development of IBD (Halfvarson et al., 2003). One might speculate that microbial- or food-derived XBP1 inhibitors could interfere with the pathways described herein, particularly in a genetically susceptible host, thus contributing to the development of intestinal inflammation. Along those lines, a recent report found that a 21-membered macrocyclic lactam termed "trierixin" isolated from Streptomyces sp. potently inhibits endogenous XBP1 splicing in an epithelial cell line (Tashiro et al., 2007).

Paneth Cell Deficiency, IEC Inflammatory Tone, and Enteritis

Although Paneth and absorptive epithelial cells have been linked to intestinal inflammation (Kobayashi et al., 2005; Zaph et al., 2007; Nenci et al., 2007; Wehkamp et al., 2005), neither Paneth cell depletion (Garabedian et al., 1997), inability to convert procryptdins to cryptdins (Wilson et al., 1999), nor *Nod2* deletion (Kobayashi et al., 2005) cause spontaneous or induced intestinal inflammation. A recent study reported development of spontaneous UC that is dependent on a specific "colitogenic" microbial milieu arising in a genetically altered host that is vertically and horizontally transmissible to genetically intact mice (Garrett et al., 2007). However, such colitogenic microbiota does not apparently arise in Paneth cell- or cryptdin-deficient mice (Garabedian et al., 1997; Wilson et al., 1999; Kobayashi et al., 2005). We conclude that bacterial "dysbiosis" alone is insufficient to cause intestinal inflammation if unaccompanied by a proinflammatory state including that primarily of the epithelium.

XBP1 deficiency in IECs resulted in IRE1α hyperactivation through an unidentified mechanism and increased JNK phosphorylation in the epithelial compartment in vivo. An increased susceptibility to DSS colitis was reported in *Ire1*$\beta^{-/-}$ mice (Bertolotti et al., 2001). Although IRE1β deficiency did not lead to spontaneous enteritis, colitis, or Paneth cell depletion, baseline levels of grp78 were elevated consistent with an active UPR in the absence of IRE1β. IECs are currently emerging as key mediators of inflammatory and immune mechanisms in mucosal tissues. IEC deletion of *Ikk*β (Zaph et al., 2007) or *Nemo* (Nenci et al., 2007), both upstream of NFκB, resulted in mucosal immune dysfunction and spontaneous colitis, respectively, the latter as a consequence of IEC barrier dysfunction. We find that even minor deficiencies in XBP1 expression within IECs lead to spontaneous enteritis, while leaving the intestinal barrier largely intact.

Genetic Association of *XBP1* Polymorphisms with IBD

IBD is a complex polygenic disease as evidenced by the recent discovery and replication of several genetic risk factors that include *NOD2*, the *5q31* haplotype (*SLC22A4*, *SLC22A5*), the *5p13.1* locus (*PTGER4*), *DLG5*, the *IL23* receptor, *ATG16L1*, *IRGM*, and *IL12B* on 5q33, *NKX2-3*, *PTPN2*, the *17q23.2* and *17q11.1* loci, and *NELL1* (Mathew, 2008). Because the functionally relevant variants for most of these loci and their role in IBD pathogenesis remain to be identified, a coherent model from gene to intestinal inflammation has yet to be developed, although some of these risk alleles point toward abnormalities of innate immune responses (e.g., *NOD2*) and autophagy (e.g., *ATG16L1*, *IRGM*), adaptive immune functions (e.g., *IL23R*), and the intestinal epithelial barrier (e.g., *DLG5*) in human IBD. Our studies reveal abnormalities of the ER stress response as another pathway for the development of intestinal inflammation and IBD.

We suggest that the linkage results obtained on chromosome 22 from three independent microsatellite-based genome scans (Hampe et al., 1999; Barmada et al., 2004; Vermeire et al., 2004) could reflect the associations of rare and common variants of the *XBP1* gene region reported here. A currently emerging concept is that rare sequence variants with strong phenotypic effects might contribute substantially to variation in complex traits, and the aggregated risk contribution may result in common traits (Cohen et al., 2004; Gorlov et al., 2008), a view strongly supported by analyzing frequencies of synonymous and nonsynonymous SNPs in an extensive data set. The authors found that the distribution of SNPs predicted to be "possibly" and "probably" damaging was shifted toward rare SNPs compared with the MAF distribution of benign and synonymous SNPs that are not likely to be functional (Gorlov et al., 2008). We found rare SNPs three times more frequently in the CD and UC sequencing cohorts than the control cohort and validated five rare nonsynonymous coding variants, four of them present only in IBD patients.

Functional studies revealed that two of these IBD-restricted nonsynonymous SNPs behaved as hypomorphs as evidenced by decreased transactivation of the UPR and induction of XBP1s target genes, either in all conditions tested (*XBP1snp8*) or in response to exogenous induction of ER stress (*XBP1snp17*). This pattern of decreased transactivation upon transfection of mutant *XBP1* cDNAs was observed in IEC lines with endogenous (wild-type) XBP1, as well as *Xbp1*$^{-/-}$ MEFs reconstituted with mutant or wild-type *XBP1*. Hence, these rare, IBD-associated variants are indeed hypomorphic, as would be predicted for risk-conferring variants from the mechanisms established through our mouse model. Whereas the functional impact of nonsynonymous SNPs can be estimated by in vitro studies as presented herein, the biological significance and contribution to disease risk of the other associated as well as rare SNPs located outside the coding region is hard to predict; nonetheless, there are excellent examples that those variants could have important functional consequences (Birney et al., 2007; Libioulle et al., 2007). The phenomenon that multiple rare variants contribute to the overall risk at a particular locus most likely represents a common situation in many complex polygenic diseases (i.e., every patient has a "private" risk SNP). This is also exemplified by *NOD2*, which not only harbors few common alleles strongly associated with CD but also multiple rare alleles that—taken together—account for a substantial proportion of disease risk attributed to that locus. It cannot be excluded though, taking the results of the haplotype analysis into account, that common variants contribute to disease risk at the *XBP1* locus in addition to the excess of private variants in patients. We assume that most given disease-associated genes will have a wide spectrum of allelic variants, both common and rare/private.

EXPERIMENTAL PROCEDURES

Mice

The generation of *Xbp1*$^{flox/flox}$*VCre* and *VCre-ER*^{T2} transgenic mice is detailed in Supplemental Data. All mouse protocols were approved by the Harvard Standing Committee on Animals.

Reagents

The sources of antibodies, proteins, and inhibitors are as follows: rabbit phospho-JNK, total-JNK, active (cleaved) caspase-3 (Cell Signaling Technology), anti-lysozyme (DakoCytomation), anti-procryptdin (Ayabe et al., 2002) generously provided by A. Ouellette (University of California, Irvine), flagellin (Invivogen), and TNFα (Peprotech). The JNK-1, -2, and -3 inhibitor SP600125 (Sigma), p38 inhibitor SB203580, and MEK inhibitors PD98059 and U0126 (Calbiochem) were dissolved in DMSO as recommended. Carbamyl choline and lipopolysaccharide (from *Escherichia coli* 0111:B4) (Sigma) were used at final concentrations of 10 μM and 1 μg/ml, respectively.

Immunohistochemistry, TUNEL, and Electron Microscopy

Tissues were handled by standard methods as detailed in Supplemental Experimental Procedures. Apoptotic cells were detected on paraffin-embedded small intestine using a TUNEL-POD kit (Roche Applied Sciences). Small intestinal tissue from sex-matched *Xbp1*$^{+/+}$ and *Xbp1*$^{-/-}$ littermates was fixed as previously described (see Supplemental Experimental Procedures) and observed with a JEOL 1200EX TEM at 60 kV operating voltage.

Oral *L. monocytogenes* Infection

Sex- and age-matched groups of *Xbp1*$^{+/+}$ and *Xbp1*$^{-/-}$ littermates were infected under BL2 conditions using gastric gavage at 3.6 × 10^8 *L. monocytogenes* strain 10403s per mouse. Colony forming unit assays (feces c.f.u./mg dry weight; liver and spleen c.f.u./organ) were performed as in Kobayashi et al. (2005) and Supplemental Experimental Procedures.

Dextran Sodium Sulfate Colitis

Sex- and age-matched littermates (8–12 weeks) received 4.5% DSS (ICN Biomedicals) in drinking water for 5 days and then regular water thereafter, or neomycin sulfate and metronidazole (1.5 g/L) (Sigma). Antibiotic-treated mice received 7% DSS. Weight was recorded daily and rectal bleeding was assessed (0, absent; 1, traces of blood at anus or the base of the tail; 2, clearly visible rectal blood). Histological and mRNA expression studies on RNeasy kit-isolated colon RNA (QIAGEN) used mice sacrificed on day 8 after DSS treatment. Histological scoring of colons was as in Garrett et al. (2007).

Crypt Isolation, Stimulation, and Bactericidal Activity Assays

Small intestinal crypts were isolated, stimulated with 10 μM CCh or 1 μg/ml LPS, and lysozyme levels and bactericidal activity against 1 × 10^3 c.f.u. *Salmonella typhimurium* cs015 were measured following published protocols (Ayabe et al., 2000) and Supplemental Experimental Procedures.

Bromodeoxyuridine Incorporation

Xbp1$^{+/+}$ and *Xbp1*$^{-/-}$ littermates were injected with 1 mg bromodeoxyuridine (BrdU; Becton Dickinson) in 500 μl PBS. Small intestinal tissue was harvested after 1 or 24 hr and paraffin-embedded tissue was sectioned and stained with anti-BrdU antibody (Becton Dickinson).

Epithelial RNA Isolation and Quantification

Xbp1$^{+/+}$ and *Xbp1*$^{-/-}$ intestines were opened longitudinally, rinsed with cold PBS, everted on a plain surface, RNAlater added, and epithelium immediately scraped off using RNase-free glass slides. Total RNA isolated using RNAeasy columns (QIAGEN) was reverse transcribed and quantified by SYBR green PCR (Bio-Rad). For microarray analysis, RNAs isolated from three specimens per genotype were pooled, and microarrays were carried out at the Biopolymers Core Facility (Harvard Medical School) with mouse genome 430 2.0 array (Affymetrix). Data analysis was performed with Agilent GeneSpring GX and Affymetrix GCOS software under default parameter setting. Quantitative PCR was performed as in Lee et al. (2003b). See Table S5 for PCR primers.

XBP1 Splicing Assay

XBP1 splicing was measured by specific primers flanking the splicing site yielding PCR product sizes of 164 and 138 bp for human XBP1u and XBP1s, and 171 and 145 bp for mouse XBP1. Products were resolved on 2% agarose gels, and band intensity was determined densitometrically (Optiquant software, Perkin Elmer).

XBP1 Silencing in MODE-K Cells

The SV40 large T-antigen-immortalized small intestinal epithelial cell line MODE-K (gift of D. Kaiserlian, Institute Pasteur) was transduced as described (Iwakoshi et al., 2003) with an XBP1-specific RNAi vector and a control vector identical to Lee et al. (2003a) except that SFGΔU3hygro was used, and knockdown was confirmed by qPCR. MODE-K.iXBP and MODE-K.Ctrl were seeded for CXCL1 experiments as described (Song et al., 1999) at 1 × 10^5 cells/well in 96-well plates, adhered for 2–4 hr, supernatant removed, and stimulated with flagellin and TNFα for 4 hr or preincubated for 30 min with JNK, p38, and MEK inhibitors, supernatants removed, and cells stimulated in fresh media with flagellin and TNFα. CD1d-restricted antigen presentation by MODE-K cells (van de Wal et al., 2003) is in Supplemental Experimental Procedures. JNK phosphorylation was assessed in MODE-K cells seeded at 1 × 10^6 per well in 6-well plates, allowed to form confluent monolayers over 48–72 hr, stimulated with flagellin and TNFα for the indicated time periods, washed in ice-cold PBS, and lysed in 500 μl RIPA buffer (50 mM Tris [pH 7.4], 150 mM NaCl, 1% Nonidet P-40, 0.5% sodium deoxycholate, 0.1% SDS) supplemented with protease (Complete, Roche Applied Science) and Ser/Thr and Tyr phosphatase (Upstate) inhibitors.

Western Blot

Protein content of lysates was determined by BCA assay, and equal amounts of lysates containing Laemmli buffer were boiled at 95°C for 5 min, resolved on 10% SDS-PAGE (for MODE-K cell lysates) or 12% SDS-PAGE (for TCA precipitates of purified crypts), transferred to Protran membranes (Whatman), blocked with 5% milk in TBS-T, incubated with primary antibody in 3%–5% BSA in TBS-T at 4°C overnight, washed, and incubated with a 1:2000 dilution of HRP-conjugated anti-rabbit secondary antibody in 3%–5% milk in TBS-T for 45 min at room temperature. Bands were visualized using SuperSignal chemiluminescent substrate (Pierce).

Human Biopsy Samples

Ileal and colonic biopsies were obtained from randomly selected patients with clinically, endoscopically, and histologically confirmed diagnosis of CD and UC, as well as healthy control patients without any signs of intestinal inflammation. The diagnosis of CD and UC was confirmed by established criteria of clinical, radiological, and endoscopic analysis, and from histology reports. Informed consent was obtained and procedures were performed according to approval by the local ethics committee of the Innsbruck Medical University. Biopsies were collected in RNAlater (Ambion), RNA was isolated using RNAeasy columns (QIAGEN), reverse transcribed, and used for quantitative PCR and XBP1 splicing assays.

Patient Recruitment

German patients and controls in panels 1 and 2 almost completely overlap with the panels termed A and B in two recently published studies (Franke et al., 2007; Hampe et al., 2007). Panel 3 is unpublished. All patients were recruited at the Charité University Hospital (Berlin, Germany) and the Department of General Internal Medicine of the Christian-Albrechts-University (Kiel, Germany), with support from the German Crohn and Colitis Foundation and BMBF competence network "IBD." Clinical, radiological, and endoscopic (i.e., type and distribution of lesions) studies unequivocally confirmed the diagnosis of CD or UC, with confirmative or compatible histological findings (Nikolaus and Schreiber, 2007). In the case of uncertainty, patients were excluded from the study. German healthy control individuals were obtained from the PopGen Biobank (Krawczak et al., 2006). Informed written consent was obtained from all study participants. All collection protocols were approved by the Charité University Hospital and the Department of General Internal Medicine of the Christian-Albrechts-University ethics committees.

Genotyping and Sequencing

Genomic DNA was prepared and amplified as in Supplemental Experimental Procedures, genotyping was performed using the SNPlex Genotyping System (Applied Biosystems) on an automated platform, genotypes were generated by automatic calling using Genemapper 4.0 software (Applied Biosystems), and all cluster plots were reviewed manually. Prior to statistical analyses, quality checks ($P_{HWE} > 0.01$, $MAF_{controls} > 1\%$, callrate $\geq 90\%$) were applied to the

SNPs under study. Single-marker association and haplotype analyses, permutation tests, calculation of pairwise LD, and SNP selection were performed using Haploview 4.0 (Barrett et al., 2005). Haplotype blocks were automatically defined as in Gabriel et al. (2002). Only haplotypes with population frequencies > 1.0% were included in the final association analysis.

Single-marker disease associations and possible marker-marker interactions were assessed for statistical significance by means of logistic regression analysis (forward selection), as implemented in the procedure LOGISTIC of the SAS software package (SAS Institute). Prior to analyses, individuals with missing data were removed and genotypes were coded numerically.

Genomic DNA sequencing was performed using BigDye chemistry (Applied Biosystems) according to the supplier's recommendations (for primer sequences, see Table S6) and analyzed as described in Supplemental Experimental Procedures. Authenticity of the five novel discovered rare nsSNPs and *rs5762809* was checked by TaqMan genotyping (Applied Biosystems) on an automated platform. For primer and probe sequences, see Tables S6 and S7; for genotype counts, see Tables S2 and S4.

UPRE Reporter Assays

Expression plasmids h*XBP1u* and h*XBP1s* were engineered to incorporate the *XBP1snp17* (A162P), *XBP1snp8* (M139I), and *XBP1snp22* (P15L) minor variants using the GeneTailor site-directed mutagenesis system (Invitrogen). See Supplemental Data for primers used. Transient transfection of MODE-K cells followed by luciferase assays was performed as in Lee et al. (2003b). Reconstitution of *Xbp1*$^{-/-}$ MEF cells was with bicistronic retroviral vectors expressing GFP and human XBP1 constructed by inserting PCR-amplified cDNAs for human wild-type and *XBP1snp17* and *XBP1snp8* variants into RV_{GFP} vector between BglII and SalI sites, as described previously (Iwakoshi et al., 2003) and transduced as described (Lee et al., 2003b).

SUPPLEMENTAL DATA

Supplemental Data include 11 figures, 7 tables, and Supplemental Experimental Procedures and can be found with this article online at http://www.cell.com/cgi/content/full/134/5/743/DC1/.

ACKNOWLEDGMENTS

We thank Drs. S. Robine and N. Davidson for V*Cre-ER*^{T2} mice; Dr. S. Ito for help with EM; Drs. J. Rioux, A. Ouelette, and M. Starnbach for helpful discussions; P. Gupta, B. Enrich, and D. Lindenbergh-Kortleve for technical support; and Dr. S. Snapper for critical reading of the manuscript. This work was supported by grants from the Crohn's and Colitis Foundation of America (R.S.B. and A.K.), NIH grants DK44319 (R.S.B.), P30 DK034854 (R.S.B.; Harvard Digestive Diseases Center), and AI32412 and P01 AI56296 (L.H.G.), the Ellison Medical Foundation (L.H.G.), CDA 1P50CA100707(A.-H.L.), the Austrian Science Fund (A.K. and H.T.), the Max Kade Foundation (A.K.), and the DFG/BMBF Excellence Cluster "Inflammation at Interfaces" (S.S. and A.F.). The authors wish to thank the patients, families, and physicians for their cooperation. The cooperativeness of the German Crohn and Colitis patient association (Deutsche Morbus Crohn und Colitis Vereinigung e.V.) and of the German "Kompetenznetz Darmerkrankungen" are gratefully acknowledged. Genotyping in this study was supported by the German Ministry of Education and Research (BMBF) through the National Genome Research Network (NGFN) and the PopGen Biobank.

Received: December 3, 2007
Revised: April 10, 2008
Accepted: July 16, 2008
Published: September 4, 2008

REFERENCES

Acosta-Alvear, D., Zhou, Y., Blais, A., Tsikitis, M., Lents, N.H., Arias, C., Lennon, C.J., Kluger, Y., and Dynlacht, B.D. (2007). XBP1 controls diverse cell type- and condition-specific transcriptional regulatory networks. Mol. Cell *27*, 53–66.

Ayabe, T., Satchell, D.P., Wilson, C.L., Parks, W.C., Selsted, M.E., and Ouellette, A.J. (2000). Secretion of microbicidal α-defensins by intestinal Paneth cells in response to bacteria. Nat. Immunol. *1*, 113–118.

Ayabe, T., Satchell, D.P., Pesendorfer, P., Tanabe, H., Wilson, C.L., Hagen, S.J., and Ouellette, A.J. (2002). Activation of Paneth cell α-defensins in mouse small intestine. J. Biol. Chem. *277*, 5219–5228.

Barker, N., van Es, J.H., Kuipers, J., Kujala, P., van den Born, M., Cozijnsen, M., Haegebarth, A., Korving, J., Begthel, H., Peters, P.J., and Clevers, H. (2007). Identification of stem cells in small intestine and colon by marker gene Lgr5. Nature *449*, 1003–1007.

Barmada, M.M., Brant, S.R., Nicolae, D.L., Achkar, J.P., Panhuysen, C.I., Bayless, T.M., Cho, J.H., and Duerr, R.H. (2004). A genome scan in 260 inflammatory bowel disease-affected relative pairs. Inflamm. Bowel Dis. *10*, 513–520.

Barrett, J.C., Fry, B., Maller, J., and Daly, M.J. (2005). Haploview: analysis and visualization of LD and haplotype maps. Bioinformatics *21*, 263–265.

Bertolotti, A., Wang, X., Novoa, I., Jungreis, R., Schlessinger, K., Cho, J.H., West, A.B., and Ron, D. (2001). Increased sensitivity to dextran sodium sulfate colitis in IRE1β-deficient mice. J. Clin. Invest. *107*, 585–593.

Birney, E., Stamatoyannopoulos, J.A., Dutta, A., Guigo, R., Gingeras, T.R., Margulies, E.H., Weng, Z., Snyder, M., Dermitzakis, E.T., Thurman, R.E., et al. (2007). Identification and analysis of functional elements in 1% of the human genome by the ENCODE pilot project. Nature *447*, 799–816.

Calfon, M., Zeng, H., Urano, F., Till, J.H., Hubbard, S.R., Harding, H.P., Clark, S.G., and Ron, D. (2002). IRE1 couples endoplasmic reticulum load to secretory capacity by processing the XBP-1 mRNA. Nature *415*, 92–96.

Cohen, J.C., Kiss, R.S., Pertsemlidis, A., Marcel, Y.L., McPherson, R., and Hobbs, H.H. (2004). Multiple rare alleles contribute to low plasma levels of HDL cholesterol. Science *305*, 869–872.

Franke, A., Hampe, J., Rosenstiel, P., Becker, C., Wagner, F., Hasler, R., Little, R.D., Huse, K., Ruether, A., Balschun, T., et al. (2007). Systematic association mapping identifies NELL1 as a novel IBD disease gene. PLoS ONE *2*, e691.

Gabriel, S.B., Schaffner, S.F., Nguyen, H., Moore, J.M., Roy, J., Blumenstiel, B., Higgins, J., DeFelice, M., Lochner, A., Faggart, M., et al. (2002). The structure of haplotype blocks in the human genome. Science *296*, 2225–2229.

Garabedian, E.M., Roberts, L.J., McNevin, M.S., and Gordon, J.I. (1997). Examining the role of Paneth cells in the small intestine by lineage ablation in transgenic mice. J. Biol. Chem. *272*, 23729–23740.

Garrett, W.S., Lord, G.M., Punit, S., Lugo-Villarino, G., Mazmanian, S.K., Ito, S., Glickman, J.N., and Glimcher, L.H. (2007). Communicable ulcerative colitis induced by T-bet deficiency in the innate immune system. Cell *131*, 33–45.

Gorlov, I.P., Gorlova, O.Y., Sunyaev, S.R., Spitz, M.R., and Amos, C.I. (2008). Shifting paradigm of association studies: value of rare single-nucleotide polymorphisms. Am. J. Hum. Genet. *82*, 100–112.

Halfvarson, J., Bodin, L., Tysk, C., Lindberg, E., and Jarnerot, G. (2003). Inflammatory bowel disease in a Swedish twin cohort: a long-term follow-up of concordance and clinical characteristics. Gastroenterology *124*, 1767–1773.

Hampe, J., Schreiber, S., Shaw, S.H., Lau, K.F., Bridger, S., MacPherson, A.J., Cardon, L.R., Sakul, H., Harris, T.J., Buckler, A., et al. (1999). A genomewide analysis provides evidence for novel linkages in inflammatory bowel disease in a large European cohort. Am. J. Hum. Genet. *64*, 808–816.

Hampe, J., Franke, A., Rosenstiel, P., Till, A., Teuber, M., Huse, K., Albrecht, M., Mayr, G., De La Vega, F.M., Briggs, J., et al. (2007). A genome-wide association scan of nonsynonymous SNPs identifies a susceptibility variant for Crohn disease in ATG16L1. Nat. Genet. *39*, 207–211.

Heazlewood, C.K., Cook, M.C., Eri, R., Price, G.R., Tauro, S.B., Taupin, D., Thornton, D.J., Png, C.W., Crockford, T.L., Cornall, R.J., et al. (2008). Aberrant mucin assembly in mice causes endoplasmic reticulum stress and spontaneous inflammation resembling ulcerative colitis. PLoS Med. *5*, e54.

Iwakoshi, N.N., Lee, A.H., Vallabhajosyula, P., Otipoby, K.L., Rajewsky, K., and Glimcher, L.H. (2003). Plasma cell differentiation and the unfolded protein response intersect at the transcription factor XBP-1. Nat. Immunol. *4*, 321–329.

Kobayashi, K.S., Chamaillard, M., Ogura, Y., Henegariu, O., Inohara, N., Nunez, G., and Flavell, R.A. (2005). Nod2-dependent regulation of innate and adaptive immunity in the intestinal tract. Science *307*, 731–734.

Kojouharoff, G., Hans, W., Obermeier, F., Mannel, D.N., Andus, T., Scholmerich, J., Gross, V., and Falk, W. (1997). Neutralization of tumour necrosis factor (TNF) but not of IL-1 reduces inflammation in chronic dextran sulphate sodium-induced colitis in mice. Clin. Exp. Immunol. *107*, 353–358.

Krawczak, M., Nikolaus, S., von Eberstein, H., Croucher, P.J., El Mokhtari, N.E., and Schreiber, S. (2006). PopGen: population-based recruitment of patients and controls for the analysis of complex genotype-phenotype relationships. Community Genet. *9*, 55–61.

Lee, A.H., Iwakoshi, N.N., Anderson, K.C., and Glimcher, L.H. (2003a). Proteasome inhibitors disrupt the unfolded protein response in myeloma cells. Proc. Natl. Acad. Sci. USA *100*, 9946–9951.

Lee, A.H., Iwakoshi, N.N., and Glimcher, L.H. (2003b). XBP-1 regulates a subset of endoplasmic reticulum resident chaperone genes in the unfolded protein response. Mol. Cell. Biol. *23*, 7448–7459.

Lee, A.H., Chu, G.C., Iwakoshi, N.N., and Glimcher, L.H. (2005). XBP-1 is required for biogenesis of cellular secretory machinery of exocrine glands. EMBO J. *24*, 4368–4380.

Libioulle, C., Louis, E., Hansoul, S., Sandor, C., Farnir, F., Franchimont, D., Vermeire, S., Dewit, O., de Vos, M., Dixon, A., et al. (2007). Novel Crohn disease locus identified by genome-wide association maps to a gene desert on 5p13.1 and modulates expression of PTGER4. PLoS Genet. *3*, e58.

Lin, J.H., Li, H., Yasumura, D., Cohen, H.R., Zhang, C., Panning, B., Shokat, K.M., Lavail, M.M., and Walter, P. (2007). IRE1 signaling affects cell fate during the unfolded protein response. Science *318*, 944–949.

Lodes, M.J., Cong, Y., Elson, C.O., Mohamath, R., Landers, C.J., Targan, S.R., Fort, M., and Hershberg, R.M. (2004). Bacterial flagellin is a dominant antigen in Crohn disease. J. Clin. Invest. *113*, 1296–1306.

Madison, B.B., Dunbar, L., Qiao, X.T., Braunstein, K., Braunstein, E., and Gumucio, D.L. (2002). Cis elements of the villin gene control expression in restricted domains of the vertical (crypt) and horizontal (duodenum, cecum) axes of the intestine. J. Biol. Chem. *277*, 33275–33283.

Mathew, C.G. (2008). New links to the pathogenesis of Crohn disease provided by genome-wide association scans. Nat. Rev. Genet. *9*, 9–14.

Nenci, A., Becker, C., Wullaert, A., Gareus, R., van Loo, G., Danese, S., Huth, M., Nikolaev, A., Neufert, C., Madison, B., et al. (2007). Epithelial NEMO links innate immunity to chronic intestinal inflammation. Nature *446*, 557–561.

Nikolaus, S., and Schreiber, S. (2007). Diagnostics of inflammatory bowel disease. Gastroenterology *336*, 1670–1689.

Reimold, A.M., Iwakoshi, N.N., Manis, J., Vallabhajosyula, P., Szomolanyi-Tsuda, E., Gravallese, E.M., Friend, D., Grusby, M.J., Alt, F., and Glimcher, L.H. (2001). Plasma cell differentiation requires the transcription factor XBP-1. Nature *412*, 300–307.

Ron, D., and Walter, P. (2007). Signal integration in the endoplasmic reticulum unfolded protein response. Nat. Rev. Mol. Cell Biol. *8*, 519–529.

Shaffer, A.L., Shapiro-Shelef, M., Iwakoshi, N.N., Lee, A.H., Qian, S.B., Zhao, H., Yu, X., Yang, L., Tan, B.K., Rosenwald, A., et al. (2004). XBP1, downstream of Blimp-1, expands the secretory apparatus and other organelles, and increases protein synthesis in plasma cell differentiation. Immunity *21*, 81–93.

Shkoda, A., Ruiz, P.A., Daniel, H., Kim, S.C., Rogler, G., Sartor, R.B., and Haller, D. (2007). Interleukin-10 blocked endoplasmic reticulum stress in intestinal epithelial cells: impact on chronic inflammation. Gastroenterology *132*, 190–207.

Song, F., Ito, K., Denning, T.L., Kuninger, D., Papaconstantinou, J., Gourley, W., Klimpel, G., Balish, E., Hokanson, J., and Ernst, P.B. (1999). Expression of the neutrophil chemokine KC in the colon of mice with enterocolitis and by intestinal epithelial cell lines: effects of flora and proinflammatory cytokines. J. Immunol. *162*, 2275–2280.

Strober, W., Fuss, I.J., and Blumberg, R.S. (2002). The immunology of mucosal models of inflammation. Annu. Rev. Immunol. *20*, 495–549.

Tashiro, E., Hironiwa, N., Kitagawa, M., Futamura, Y., Suzuki, S., Nishio, M., and Imoto, M. (2007). Trierixin, a novel inhibitor of ER stress-induced XBP1 activation from Streptomyces sp. J. Antibiot. (Tokyo) *60*, 547–553.

Urano, F., Wang, X., Bertolotti, A., Zhang, Y., Chung, P., Harding, H.P., and Ron, D. (2000). Coupling of stress in the ER to activation of JNK protein kinases by transmembrane protein kinase IRE1. Science *287*, 664–666.

van de Wal, Y., Corazza, N., Allez, M., Mayer, L.F., Iijima, H., Ryan, M., Cornwall, S., Kaiserlian, D., Hershberg, R., Koezuka, Y., et al. (2003). Delineation of a CD1d-restricted antigen presentation pathway associated with human and mouse intestinal epithelial cells. Gastroenterology *124*, 1420–1431.

Vermeire, S., Rutgeerts, P., Van Steen, K., Joossens, S., Claessens, G., Pierik, M., Peeters, M., and Vlietinck, R. (2004). Genome wide scan in a Flemish inflammatory bowel disease population: support for the IBD4 locus, population heterogeneity, and epistasis. Gut *53*, 980–986.

Wehkamp, J., Salzman, N.H., Porter, E., Nuding, S., Weichenthal, M., Petras, R.E., Shen, B., Schaeffeler, E., Schwab, M., Linzmeier, R., et al. (2005). Reduced Paneth cell α-defensins in ileal Crohn's disease. Proc. Natl. Acad. Sci. USA *102*, 18129–18134.

Wilson, C.L., Ouellette, A.J., Satchell, D.P., Ayabe, T., Lopez-Boado, Y.S., Stratman, J.L., Hultgren, S.J., Matrisian, L.M., and Parks, W.C. (1999). Regulation of intestinal α-defensin activation by the metalloproteinase matrilysin in innate host defense. Science *286*, 113–117.

Wu, J., and Kaufman, R.J. (2006). From acute ER stress to physiological roles of the unfolded protein response. Cell Death Differ. *13*, 374–384.

Zaph, C., Troy, A.E., Taylor, B.C., Berman-Booty, L.D., Guild, K.J., Du, Y., Yost, E.A., Gruber, A.D., May, M.J., Greten, F.R., et al. (2007). Epithelial-cell-intrinsic IKK-β expression regulates intestinal immune homeostasis. Nature *446*, 552–556.